ACADEMIC PRESS

Available online at www.sciencedirect.com
SCIENCE DIRECT®

Journal of Solid State Chemistry 173 (2003) 319–327

JOURNAL OF SOLID STATE CHEMISTRY

http://elsevier.com/locate/jssc

Structural analysis of several W(VI) and Mo(VI) complex perovskites prepared by the polymeric precursors method

Antonio F. Fuentes,[a,*] O. Hernández-Ibarra,[a] G. Mendoza-Suarez,[a] J.I. Escalante-García,[a] Khalid Boulahya,[b] and U. Amador[c]

[a] *CINVESTAV-IPN Unidad Saltillo, Apartado Postal 663, 25000 Saltillo, Coahuila, Mexico*
[b] *Departamento de Química Inorgánica, Facultad de Ciencias Químicas, Universidad Complutense, 28040 Madrid, Spain*
[c] *Departamento de CC. Químicas, Facultad de Ciencias Experimentales y de la Salud, Universidad San Pablo-CEU, Urbanización Montepríncipe, 28668 Boadilla del Monte, Madrid, Spain*

Received 18 November 2002; received in revised form 23 January 2003; accepted 1 February 2003

Abstract

We describe in this work the synthesis by the Pechini method of five Mo(VI)- and W(VI)-containing complex perovskites and their structural characterisation by HREM and XRD. The compounds studied, $Ba(B'_{2/3}B''_{1/3})O_3$ (B' = In and Y; B'' = W and Mo) and $Sr(In_{2/3}W_{1/3})O_3$, were obtained after firing the precursor powders for 8 h at 1200°C. Thermal analysis showed that the formation mechanism of the five perovskites is similar and implies the formation of barium carbonate and barium tungstates or molybdates of different stoichiometries as intermediate phases. Interesting enough, these similar mechanisms yield to materials of a quite different structure. Indeed, $Ba(In_{2/3}Mo_{1/3})O_3$ and $Sr(In_{2/3}W_{1/3})O_3$ were found to be disordered perovskites (unit cells: $a_p \times a_p \times a_p$ and $\sqrt{2}a_p \times \sqrt{2}a_p \times 2a_p$, respectively); on the other hand, two phases coexist in the sample $Ba(In_{2/3}W_{1/3})O_3$ at the synthesis conditions: an ordered predominant phase (unit cell: $2a_p \times 2a_p \times 2a_p$) and, as a minor phase, a disordered perovskite (unit cell: $a_p \times a_p \times a_p$). Finally, the two yttrium-containing compounds were found to be ordered perovskites ($2a_p \times 2a_p \times 2a_p$).

Keywords: Complex perovskites; Order–disorder; HREM; Tungsten (VI); Molybdenum (VI)

1. Introduction

Complex perovskites have recently attracted much attention in different areas of materials science because of their unusual and, frequently, interesting physical properties. In ABO_3 perovskites, the B ions, octahedrally coordinated, usually determine the physical properties. Therefore, it is not surprising that complex perovskites featuring two different ions sharing the B sites, such as $A(B'_{1/2}B''_{1/2})O_3$ or $A(B'_{2/3}B''_{1/3})O_3$, very often display interesting electrical and magnetic properties [1–3]. The properties of this type of compounds may be strongly affected by the order–disorder phenomena, mainly involving the B ions. It is generally accepted that ordering in complex perovskites is favoured by large differences in charge between the two B ions and by large differences in ionic radii [4]. Ionisation potentials [5], cation coordination geometry and the A-cation/B-cation size ratio [6] have been also mentioned as factors that influence the degree of ordering.

Although many compounds of this type have been investigated in recent years and their structural characteristics determined, information about $A(B'_{2/3}B''_{1/3})O_3$ materials where B'' = W(VI) or Mo(VI), remains scarce. The best known example of this type of oxide is, probably, $Pb(Fe_{2/3}W_{1/3})O_3$ (PFW), a PMN type of relaxor which presents a random distribution of Fe(III) and W(VI) over the octahedral sites. Two of the perovskites studied in this work, $Ba(Y_{2/3}W_{1/3})O_3$ and $Ba(Y_{2/3}Mo_{1/3})O_3$, are used in electrolamp industry as electron-emissive materials for gas-discharge light sources with high vapor pressure [7,8]; however, the available structural data are confusing. Some other examples of W(VI) or Mo(VI) triple perovskites studied in the literature include [9,10] $Sr(Cr_{2/3}W_{1/3})O_3$ and $Sr(Fe_{2/3}W_{1/3})O_3$, both of cubic symmetry and unit cell parameters 7.812 and 7.888 Å, respectively, and the hexagonal $Ba(Fe_{2/3}W_{1/3})O_3$ ($a = 5.770$ Å and $c = 14.140$ Å).

*Corresponding author. Fax: +52-844-4389610.
E-mail address: afernand@saltillo.cinvestav.mx (A.F. Fuentes).

0022-4596/03/$ - see front matter
doi:10.1016/S0022-4596(03)00105-1

The main purpose of this work is to determine the structural characteristics of several complex perovskites containing hexavalent tungsten or molybdenum and to show the usefulness of the Pechini method [11] as a synthesis route for complex oxides.

2. Experimental

The synthesis of the title compounds was carried out by the Pechini method, also known as the complex polymeric precursors method. This method was selected because, starting from solution, it leads to a more homogeneous mixing and to more reactive forms of the starting reagents, minimising phase segregation comparing to the traditional solid-state reaction. As starting reagents, we used: barium carbonate ($BaCO_3$, 99.98%), strontium nitrate ($Sr(NO_3)_2$, 99%), hydrated indium and yttrium nitrates (99.9%), ammonium dimolybdate and ammonium tungsten oxide [$(NH_4)_{10}W_{12}O_{41} \cdot 5H_2O$, 99.999%]. Most of these chemicals were used as supplied, except ammonium dimolybdate. This was decomposed to pure MoO_3, by firing for 12 h at 700°C, to determine its molybdenum content. After weighting the appropriate quantities to obtain $A(B^{III}_{2/3}B^{VI}_{1/3})O_3$, the starting reagents were dissolved in an aqueous solution of citric acid (CA, 99.5%) under constant stirring and heated at 80°C until a transparent solution was obtained. Then, ethylene glycol (EG, 99 + %) was added to promote the polymerisation of the metal citrates by a polyesterification reaction; while stirring, the solutions were slowly heated to 90–100°C and treated at this temperature until the almost complete removal of water. The clear gels obtained were transferred to an electrical furnace and dried at 150°C for 5 h, yielding solid resins of high porosity. The molar $CA/(A + B^{III} + B^{VI})$ ratio used for all the solutions was kept at 1.5 whereas the CA/EG ratio was maintained at unity as suggested by Lessing and Tai to obtain the most porous resins [12]. These resins were ground in an agate mortar and heated at 1200°C (heating rate 10°C/min) for 16 h in high alumina crucibles (Coors Inc.). In order to gain understanding about the formation mechanisms of the title perovskites, two kinds of experiments were performed. First, portions of the solid resins were treated in air at several temperatures ranging from 500°C to 1200°C for different holding times, followed by natural furnace cooling to room temperature. The evolution of the samples was followed by X-ray powder diffraction (XRD) on a Philips X'Pert diffractometer equipped with Cu$K\alpha$ radiation (1.5418 Å) and a nickel filter. Second, thermal analysis were carried out in a Perkin-Elmer TGA 7/PC and a Perkin-Elmer TAC/DX, using a typical sample size of approximately 10 mg, a heating rate of 10°C/min and a static air atmosphere.

XRD patterns were analysed by the Rietveld method, using the FULLPROF program [13]. Selected area electron diffraction (SAED) and high-resolution electron microscopy (HREM) were performed on a Jeol 2000FX and a Jeol 4000EX electron microscope, respectively. Local composition was determined on many crystals with an EDAX analyser system attached to the latter microscope.

3. Results and discussion

3.1. Synthesis

Powder X-ray diffraction patterns of the obtained powders revealed the formation of a perovskite-type oxide as a major phase. Small amounts of barium or strontium tungstates or molybdates of different stoichiometries, and in some cases the simple oxide of the trivalent ion (Y_2O_3 or In_2O_3), were also present as impurities. The amounts of secondary phases are higher in the strontium-containing sample.

One of the disadvantages of the Pechini method is the large weight loss produced on firing the precursors, due, basically, to the decomposition and combustion of the organic reagents used to prepare the polymeric resins (CA and EG). Weight losses depend very much on the CE + EG/metal ratio used. In our case, the five resins obtained after drying the gels at 150°C were examined by thermal analysis. All of them show a similar behaviour, with total losses of around 80% of the initial weight. As an example, Fig. 1 shows typical TGA curves for $Ba(In_{2/3}W_{1/3})O_3$ and $Sr(In_{2/3}W_{1/3})O_3$ precursors heated in air at a heating rate of 5°C/min. Almost 50% of the initial weight is lost below 300°C with a further loss of 30% between 300°C and 500°C. Slope changes above 300°C suggest the formation of well-defined intermediate products. Above 500°C only residual losses are observed (about 3–4% of the initial weight of the solid resin). This suggests that the decomposition of the organic products and the subsequent combustion have finished at that temperature. Thus, the five resins obtained were fired at 500°C to eliminate the organic matter; the resulting powders were characterised by thermal analysis and X-ray powder diffraction.

Surprisingly, the five samples showed a similar evolution with temperature: a loss of around 10% of the initial weight and a series of endothermic and exothermic events at similar temperatures. As an example, only the data corresponding to samples $Ba(In_{2/3}W_{1/3})O_3$ and $Ba(Y_{2/3}Mo_{1/3})O_3$ will be shown (Fig. 2) in the understanding that the results obtained for the remaining samples are similar. Two prominent thermal events can be noticed: one exothermic around 660°C and an endothermic one at a temperature close to

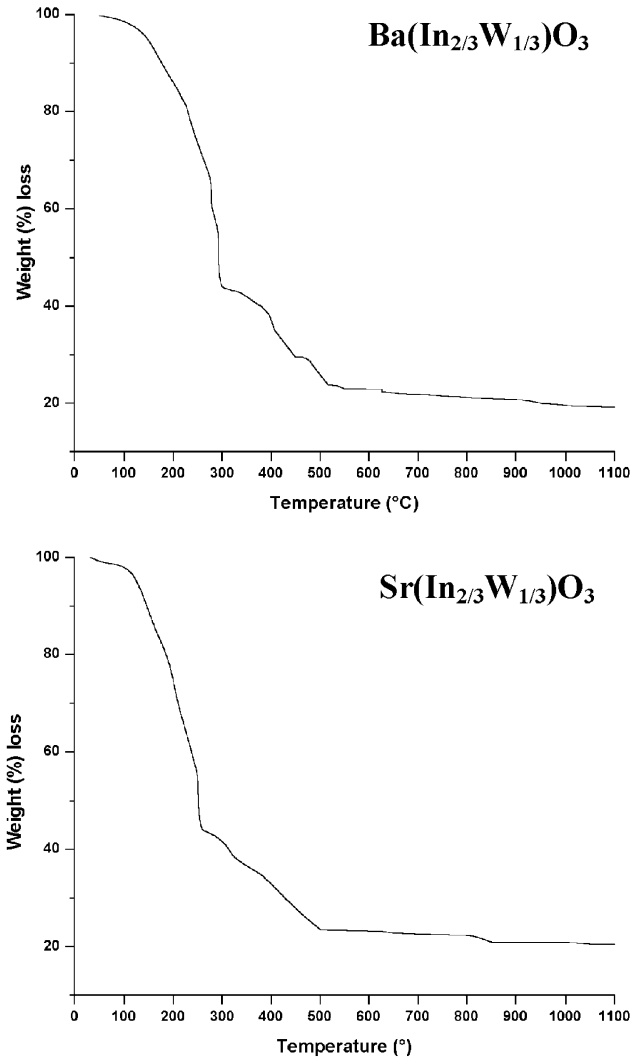

Fig. 1. TGA curves from room temperature to 1200°C, obtained for two of the precursors, $Ba(In_{2/3}W_{1/3})O_3$ and $Sr(In_{2/3}W_{1/3})O_3$ (heating rate 10°C/min).

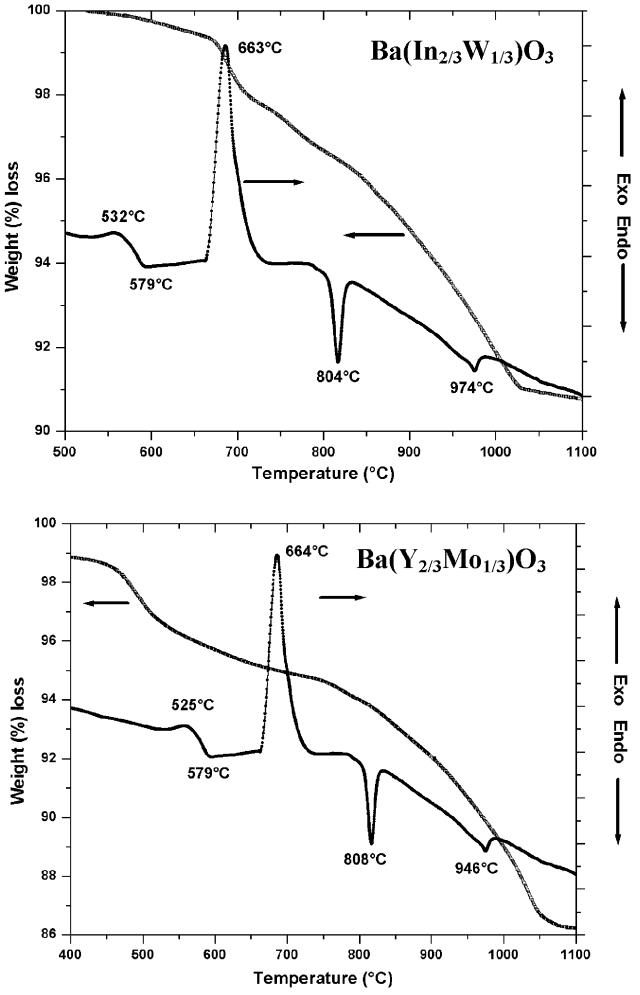

Fig. 2. Thermal analysis curves, DTA and TGA, obtained for two of the precursors, $Ba(In_{2/3}W_{1/3})O_3$ and $Ba(Y_{2/3}W_{1/3})O_3$, fired previously for 5 h at 500°C.

800°C. Additionally, there are a certain number of minor thermal events at around 530°C (exothermic), 580°C (endothermic) and 950°C (endothermic). These results indicate that the formation mechanism of the five complex perovskites prepared in this work seems to be similar. In order to identify the intermediate phases, portions of the powders were fired at different temperatures and characterised by X-ray diffraction. Fig. 3 shows the evolution with temperature of two of the precursors, $Ba(In_{2/3}W_{1/3})O_3$ and $Ba(Y_{2/3}W_{1/3})O_3$. $BaCO_3$ and $BaWO_4$ are the main crystalline phases present in the precursor containing Ba, In and W and fired at 500°C (Fig. 3a). Additionally, the presence of In_2O_3 could also be noticed, though its most intense reflection overlaps with that of a barium tungstate, $Ba_3W_2O_9$. At higher temperatures, barium tungstate ($BaWO_4$), with a Ba/W ratio of 1, transforms into tungstates with higher Ba/W ratios. Thus, $Ba_3W_2O_9$ (Ba/W = 1.5) is observed at 680°C and 800°C; Ba_2WO_5 (Ba/W = 2) is present at 680°C, 800°C and 1100°C; and Ba_3WO_6 (Ba/W = 3) is formed above 800°C. It is obvious that the formation of barium tungstates with high barium contents is related with the increasing amounts of this element available in the precursor powders as barium carbonate decomposes as the temperature is raised. The XRD pattern corresponding to the powder fired at 1100°C already shows the characteristic reflections of a perovskite-like oxide. It is worth remarking that chemical reactions involving indium atoms seem to take place only above 1000°C. This seems to be a common feature of all the precursors since no crystalline intermediate phases containing the trivalent elements are formed. Further heating produces a powder composed by a perovskite phase plus a small amount of Ba_3WO_6.

X-ray powder diffraction patterns showed no significant differences for the $Ba(Y_{2/3}W_{1/3})O_3$ precursor fired at 500°C, 700°C and 820°C (Fig. 3b). Again,

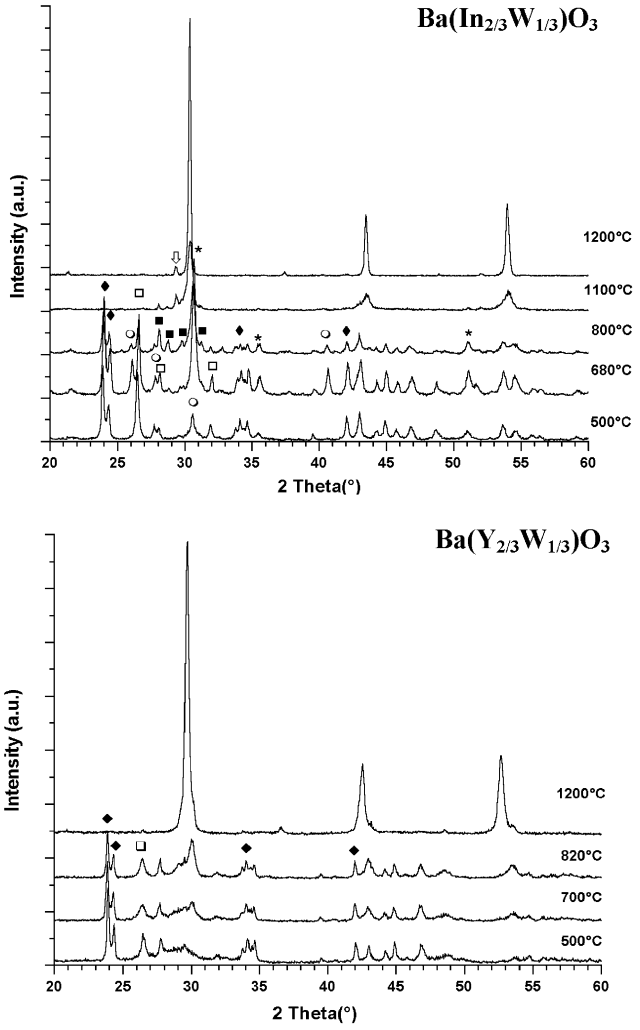

Fig. 3. Evolution of powder X-ray diffraction patterns of $Ba(In_{2/3}W_{1/3})O_3$ (a) and $Ba(Y_{2/3}W_{1/3})O_3$ (b) with temperature. (a) $BaCO_3$ (◆), $BaWO_4$ (□) and $Ba_3W_2O_9$ (○) are observed at low temperatures. Additional tungstates [Ba_2WO_5 (■) and Ba_3WO_6 (⇩)] are found when increasing the firing temperature as well as In_2O_3 (*). Barium carbonate decomposes around 900°C observing then, the formation of a perovskite-like phase. (b) $BaCO_3$ (◆) and $BaWO_4$ (□) were identified in the samples fired below 1000°C with similar powder patterns. Perovskite formation is evident for that powder fired at 1200°C.

$BaCO_3$ and $BaWO_4$ are the main crystalline phases present and no evidence is found of the existence of any crystalline compound involving the trivalent element. At 1200°C, the formation of a perovskite-like phase is clear which becomes more crystalline as the time of firing increases.

All powders were subjected to further firings at the same temperature until complete removal of undesired phases or until no changes were observed in the diffraction patterns collected after two consecutive thermal treatments. The three tungsten-containing perovskites are white coloured, while the remaining two are yellow coloured.

3.2. Structural characterisation

Published data about the structures of the title compounds are scarce and confusing. As a first approach, the Goldschmidt's tolerance factors (t) were calculated for these complex perovskites using the ionic radii given by Shannon [14]. For the B positions occupied by two ions, an average radius was used, calculated as follows: $R_B = (2R_{M(III)} + R_{M(VI)})/3$. The t values can be used as a guide to predict the crystal symmetry of a perovskite oxide, though it usefulness is limited due to its pure geometrical nature. Accordingly, the barium-containing compounds studied here would be cubic (t ranges from 0.967 to 0.999) with a structure close to the ideal perovskite, whereas for $Sr(In_{2/3}W_{1/3})O_3$, the t parameter (0.941) falls on the border between the cubic and the orthorhombic symmetries. After a literature review, we found only few papers dealing with these perovskites. Thus, Hikichi and Suzuki [15] studied several barium- and tungsten-containing perovskites, including that with Y, and concluded that $Ba(Y_{2/3}W_{1/3})O_3$ was cubic ($a = 4.258$ Å). Only after firing the sample above 1400°C, the existence of a superstructure became evident. Balashov et al. [16] proposed for this phase the existence of a cubic ($a = 8.3817$ Å) and a tetragonal form ($a = b = 6.013$ Å; $c = 4.253$ Å), though no data about possible space groups were given. Galasso [17] proposed for $Ba(In_{2/3}W_{1/3})O_3$ and $Ba(Y_{2/3}W_{1/3})O_3$ a structure similar to that of $(NH_4)_3FeF_6$ with doubled a_p ($a_p \sim 4$ Å) cell parameters (8.321 and 8.374 Å, respectively). Finally, Vrugt et al. [18] studied $Ba(Y_{2/3}Mo_{1/3})O_3$ suggesting that it has a cubic structure (S.G.: $Pm3m$) with a cell parameter of 4.261 Å. XRD was the main technique used in these works to elucidate the structure of these oxides. No published structural data were found about the remaining two perovskites studied in this paper: $Ba(In_{2/3}Mo_{1/3})O_3$ and $Sr(In_{2/3}W_{1/3})O_3$.

As a first approach, two simple models can be proposed for the structure of complex perovskite-like compounds: a complete disordered structure (i.e., with unit cell $a_p \times a_p \times a_p$ and cubic symmetry, S.G.: Pm-$3m$) with a random distribution of cations over the octahedral sites, and a complete ordered superstructure (unit cell $2a_p \times 2a_p \times 2a_p$, S.G.: Fm-$3m$).

However, things are more complex and interesting. Very often, the sole use of X-ray diffraction does not allow developing a complete structural model for complex materials. The use of electron diffraction and microscopy is mandatory, even if single crystals are available [19], to achieve a correct structural model. Thus, in our case, the complementary information provided by SAED and HREM was also used.

Thus, the SAED study of $Ba(In_{2/3}Mo_{1/3})O_3$ is shown in Fig. 4. All the observed reflections can be indexed in the basic cubic perovskite cell parameters. As no

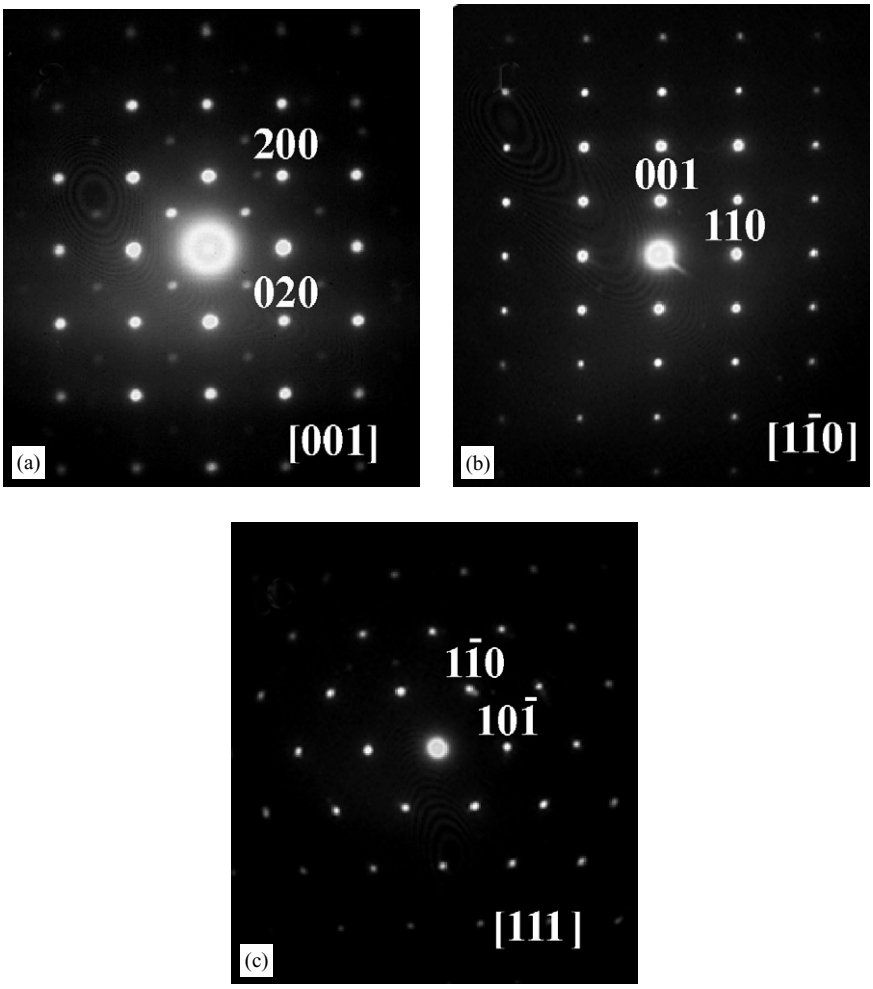

Fig. 4. SAED patterns corresponding to $Ba(In_{2/3}Mo_{1/3})O_3$, taken along [001] (a), [1−10] (b) and [111] (c). The indexing refers to a simple cubic unit cell $a_p \times a_p \times a_p$ (a_p is the unit cell parameter of the ideal perovskite).

additional maxima were observed, reflections are indexed according to a cubic unit cell $a_p \times a_p \times a_p$, where a_p is the unit cell of the ideal simple perovskite.

The SAED study of $Ba(Y_{2/3}Mo_{1/3})O_3$ is shown in Fig. 5. The strong reflections correspond to a basic cubic perovskite cell. Additional weak peaks are observed along the $[111]_c$ direction, and equivalent ones, leading to a double perovskite structure. Therefore, reflections are indexed according to the double cubic perovskite unit cell $2a_p \times 2a_p \times 2a_p$.

The SAED study of $Ba(In_{2/3}W_{1/3})O_3$, reveals two types of crystals. The first one corresponds to a basic cubic perovskite as observed for $Ba(In_{2/3}Mo_{1/3})O_3$ (Fig. 4), whereas the second type of crystals corresponds to a double perovskite unit cell, isostructural to $Ba(Y_{2/3}Mo_{1/3})O_3$ (Fig. 5).

The microstructure of $Sr(In_{2/3}W_{1/3})O_3$ is much more complex than that of the two above-described samples. Thus, in Fig. 6, the SAED study of this material is shown. Although the observed spots can be indexed on the basis of a double cubic perovskite unit cell, the corresponding high-resolution image, shown in Fig. 7, suggests a different situation. A careful analysis of the HREM image reveals the coexistence of three domains (A, B and C). Fast Fourier transform (FFT) in the three domains is shown in Figs. 7a–c. The first one corresponds to the [001] direction, whereas the second and the third ones correspond to [1−10] and the equivalent direction. Thus, the real unit cell for this phase is $\sqrt{2}a_p \times \sqrt{2}a_p \times 2a_p$.

According to the SAED and HREM results, the simplest model (simple cubic perovskite with S.G. *Pm*-3*m*) is adequate for $Ba(In_{2/3}Mo_{1/3})O_3$, whereas the situation is slightly more complex for $Ba(In_{2/3}W_{1/3})O_3$. In the latter case, crystals of the same composition (close to the nominal one, as determined by EDS on the same crystals studied by SAED) have been found showing different unit cell and symmetry. Indeed, both a disordered phase ($a = a_p$, S.G.: *Pm*-3*m*) and an ordered one ($a = 2a_p$, S.G.: *Fm*-3*m*) coexist. The case of $Sr(In_{2/3}W_{1/3})O_3$ is completely different since the symmetry of this phase is orthorhombic (S.G. *Pnma*)

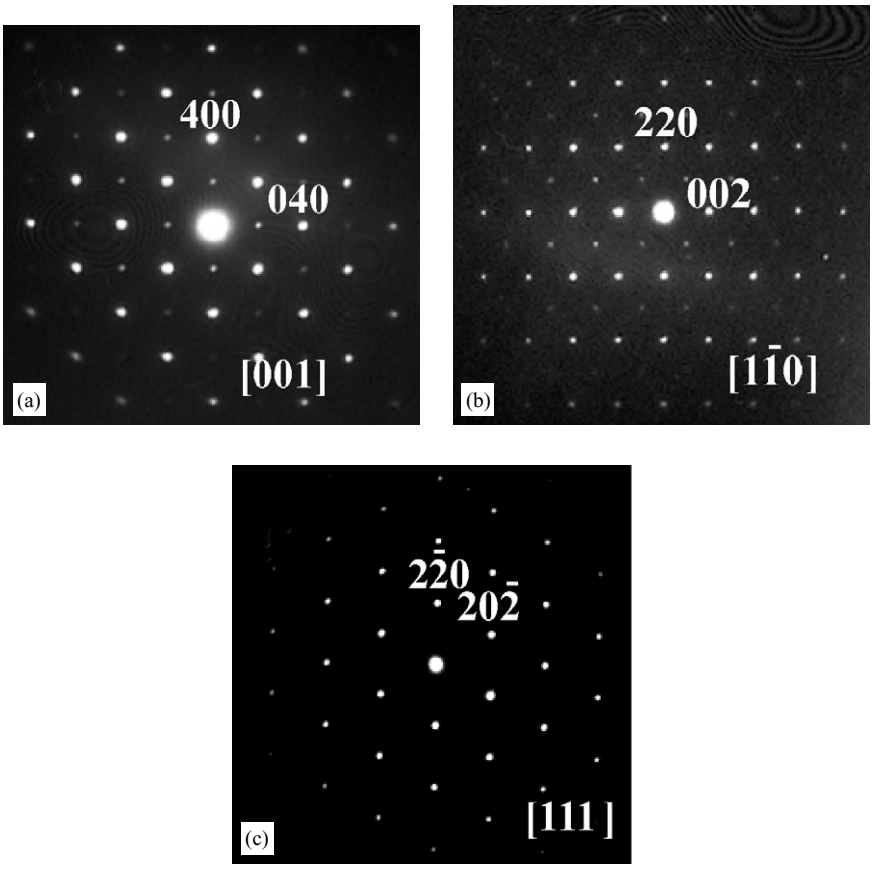

Fig. 5. SAED patterns corresponding to $Ba(Y_{2/3}Mo_{1/3})O_3$ (those ones for $Ba(Y_{2/3}W_{1/3})O_3$ are identical). (a) Pattern taken along [001], (b) pattern along [1−10], (c) pattern taken along [111]. All the maxima can be indexed on the basis of a face-centred cubic perovskite with unit cell $2a_p \times 2a_p \times 2a_p$.

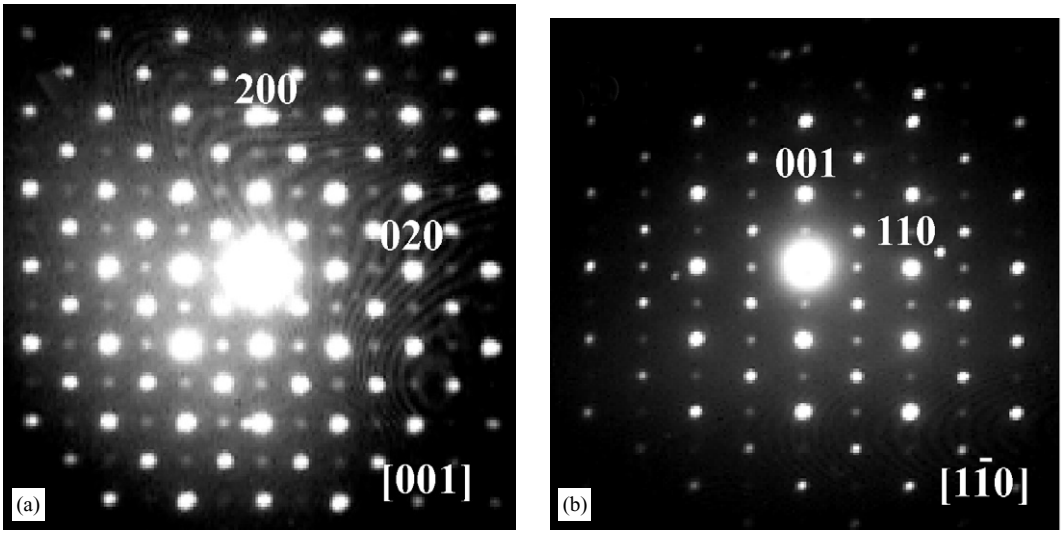

Fig. 6. SAED patterns corresponding to $Sr(In_{2/3}W_{1/3})O_3$, taken along [001] (a), and [1−10] (b). The indexing refers to a simple cubic unit cell $a_p \times a_p \times a_p$.

with unit cell $\sqrt{2}a_p \times 2a_p \times \sqrt{2}a_p$. On the other hand, both $Ba(Y_{2/3}Mo_{1/3})O_3$ and $Ba(Y_{2/3}W_{1/3})O_3$ show a double cubic cell, the symmetry being *Fm*-3*m*.

The structural models used to fit the experimental XRD data were developed on the basis of the SAED and HREM results described above. At this point, it is

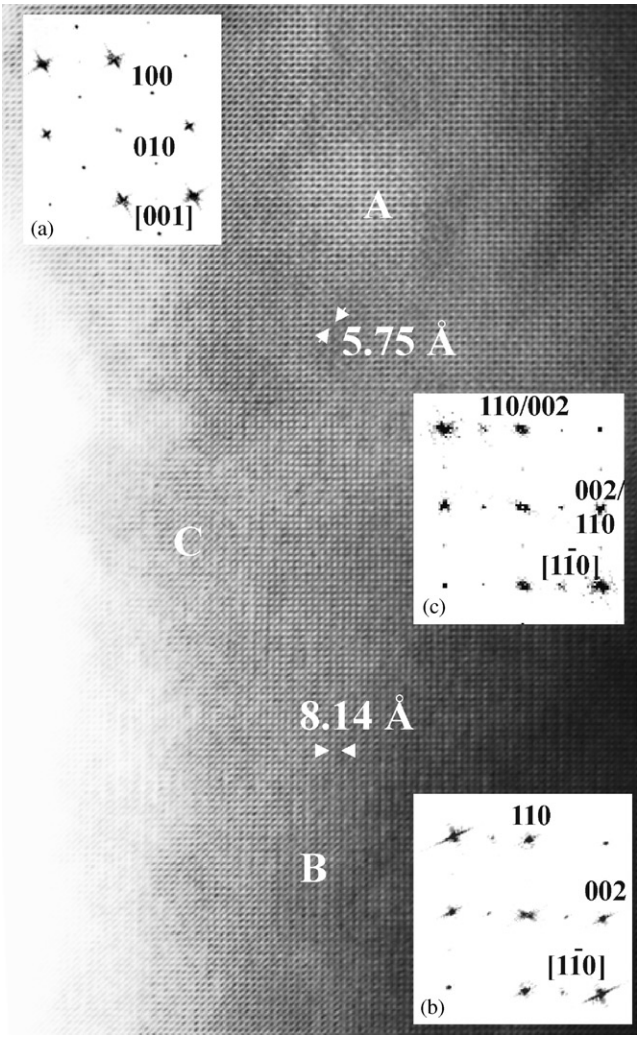

Fig. 7. HREM image of $Sr(In_{2/3}W_{1/3})O_3$ along [001]. A twinned structure is clearly seen; (a–c) are optical FFTs of the domains marked A, B and C in the image, respectively.

worth remarking that EDS analysis performed on crystals of the perovskite-like phases revealed that their actual compositions are, in every case, close to the nominal ones, in spite of the presence in the samples of small amounts of impurity phases.

Fig. 8 depicts prototypical XRD patterns for the title compounds; the observed, calculated and difference XRD powder patterns are shown. Tick marks indicate in every case the reflection positions for the perovskites and the impurity phases. In the insets of Fig. 8, schematic representations of the structures are presented. The structural parameters for all the materials are collected in Table 1, whereas Table 2 shows some selected interatomic distances.

As it was mentioned before, large differences in charge and ionic radii in perovskites drive crystal structures towards an ordered state. Regarding double perovskites, Anderson et al. [6], from structural data of more than 300 $A'A''B'B''O_6$ compounds, concluded that

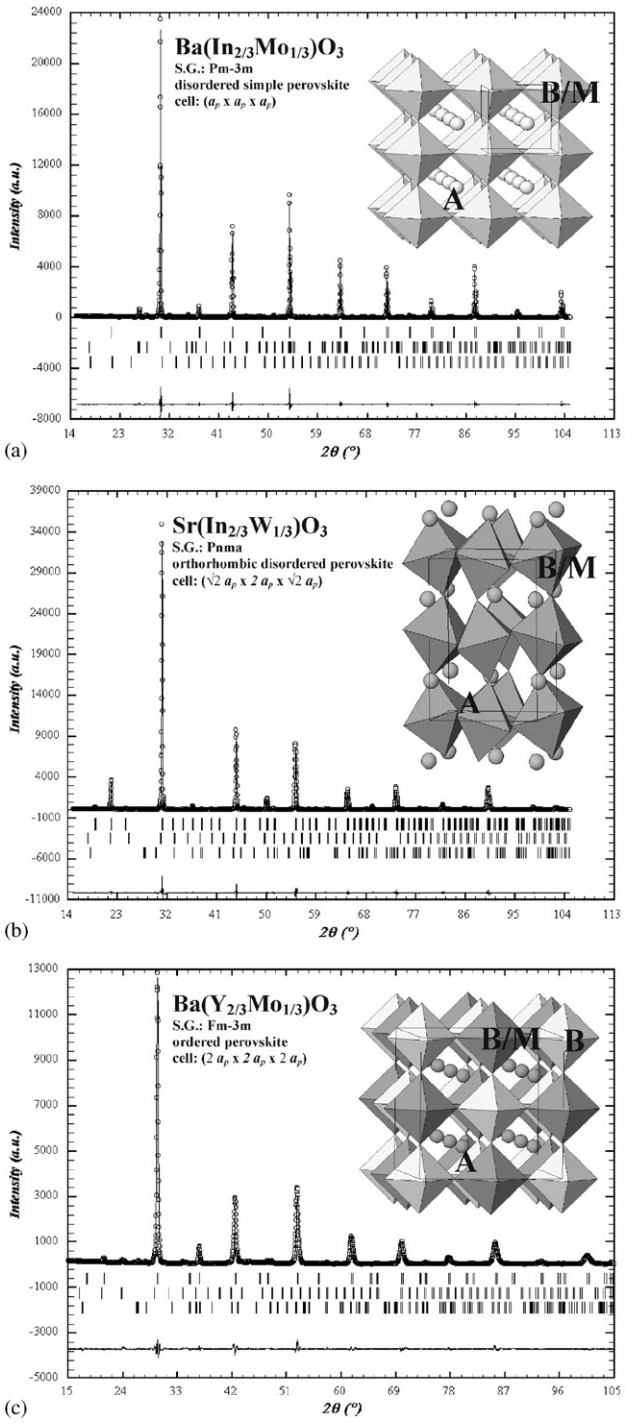

Fig. 8. Prototypical XRD patterns for the different symmetries found in perovskite-like compounds. A schematic representation of the corresponding structure is depicted. (a) Experimental (circles) and calculated XRD patterns, and their difference, for $Ba(In_{2/3}Mo_{1/3})O_3$. Vertical marks indicate the peaks of the phases present in the sample: first row $Ba(In_{2/3}Mo_{1/3})O_3$, second row $BaMoO_4$, third row In_2O_3. (b) Experimental (circles) and calculated XRD patterns, and their difference, for $Sr(In_{2/3}W_{1/3})O_3$. Vertical marks indicate the peaks of the phases present in the sample: first row $Sr(In_{2/3}W_{1/3})O_3$, second row In_2O_3, third row $SrWO_4$. (c) Experimental (circles) and calculated XRD patterns, and their difference, for $Ba(Y_{2/3}Mo_{1/3})O_3$. Vertical marks indicate the peaks of the phases present in the sample: first row $Ba(Y_{2/3}Mo_{1/3})O_3$, second row Y_2O_3, third row $BaMoO_4$.

Table 1
Final structural parameters of $A(B_{2/3}M_{1/3})O_3$ compounds

Atom	A	B	B/M	O(1)	O(2)
$Ba(In_{2/3}Mo_{1/3})O_3$[a] *(A=Ba, B=In, M=Mo)*					
x/a	1/2		0	1/2	
y/b	1/2		0	0	
z/c	1/2		0	0	
B_{iso} (A^2)	0.36(4)		0.10(5)	0.7(1)	
Occ	1		2/3:1/3	3	
$Ba(In_{2/3}W_{1/3})O_3$[b] *(A=Ba, B=In, M=W)*					
x/a	1/4	0	1/2	0.256(2)	
y/b	1/4	0	1/2	0	
z/c	1/4	0	1/2	0	
B_{iso} (A^2)	0.10(5)	0.10(4)	0.10(4)	0.16(4)	
Occ	1	3/6	1/6:2/6	3	
x/a	1/2		0	1/2	
y/b	1/2		0	0	
z/c	1/2		0	0	
B_{iso} (A^2)	0.15(2)		0.10(3)	0.3(1)	
Occ	1		2/3:1/3	3	
$Sr(In_{2/3}W_{1/3})O_3$[c] *(A=Sr, B=In, M=W)*					
x/a	0.0245(3)		0	0.484(2)	0.245(4)
y/b	1/4		0	1/4	0.047(2)
z/c	−0.0168(5)		1/2	0.053(3)	−0.290(3)
B_{iso}(A^2)	1.51(4)		0.69(2)	1.9(7)	4.1(6)
Occ	1		2/3:1/3	1	2
$Ba(Y_{2/3}Mo_{1/3})O_3$[d] *(A=Ba, B=Y, M=Mo)*					
x/a	1/4	0	1/2	0.2452(5)	
y/b	1/4	0	1/2	0	
z/c	1/4	0	1/2	0	
B_{iso} (A^2)	0.64(3)	0.28(2)	0.28(2)	2.4(2)	
Occ	1	3/6	1/6:2/6	3	
$Ba(Y_{2/3}W_{1/3})O_3$[e] *(A=Ba, B=Y, M=W)*					
x/a	1/4	0	1/2	0.2347(9)	
y/b	1/4	0	1/2	0	
z/c	1/4	0	1/2	0	
B_{iso} (A^2)	0.10(4)	0.80(5)	0.80(5)	4.4(4)	
Occ	1	3/6	1/6:2/6	3	

[a] For $Ba(In_{2/3}Mo_{1/3})O_3$, S.G. *Pm-3m* (*n*.221), $a = 4.16606(3)$ Å, $V = 72.306(2)$ Å^3, $R_B = 0.03$, $R_{exp} = 0.085$, $R_{wp} = 0.143$, $\chi^2 = 2.9$.

[b] For $Ba(In_{2/3}W_{1/3})O_3$, ordered phase (70% weight): S.G. *Fm-3m* (*n*.225), $a = 8.3150(2)$ Å, $V = 574.90(2)$ Å^3, $R_B = 0.054$, $R_{exp} = 0.087$, $R_{wp} = 0.148$, $\chi^2 = 2.9$; disordered phase (21% weight): S.G. *Pm-3m* (*n*.221), $a = 4.1573(1)$ Å, $V = 71.85(1)$ Å^3, $R_B = 0.043$.

[c] For $Sr(In_{2/3}W_{1/3})O_3$, S.G. *Pnma* (*n*.62), $a = 5.7673(2)$ Å, $b = 8.1413(3)$ Å, $c = 5.7541(2)$ Å, $V = 270.18(2)$ Å^3, $R_B = 0.09$, $R_{exp} = 0.066$, $R_{wp} = 0.15$, $\chi^2 = 5.1$.

[d] For $Ba(Y_{2/3}Mo_{1/3})O_3$, S.G. *Fm-3m*(*n*.225), $a = 8.5017(2)$ Å, $V = 614.50(3)$ Å^3, $R_B = 0.02$, $R_{exp} = 0.075$, $R_{wp} = 0.112$, $\chi^2 = 2.2$.

[e] For $Ba(Y_{2/3}W_{1/3})O_3$, S.G. *Fm-3m*(*n*.225), $a = 8.5093(3)$ Å, $V = 616.14(4)$ Å^3, $R_B = 0.06$, $R_{exp} = 0.074$, $R_{wp} = 0.206$, $\chi^2 = 7.8$.

an ordered distribution of cations was dominant when the charge difference was greater than two; otherwise the structure is disordered. A charge-difference versus ionic-radii-difference plot revealed that only when the charge difference is two and the ionic-radii difference less than 0.2 Å, both random and ordered sublattices exist. According to their data, only one compound with a charge difference of +3, $SrLaCuRuO_6$, was found to present a random distribution of cations. For the title compounds, the difference in charge between B' and B'' is +3, whereas the differences in ionic radii are 0.2 Å for the In(III)-containing and 0.3 Å for the Y(III)-containing perovskite. Therefore, one should expect an ordered cation distribution in these complex oxides. Surprisingly, as already shown, In-containing oxides were found to present a random distribution of cations over the octahedral site. Obviously, the criteria mentioned above, though generally fulfilled, have exceptions; some complex perovskites have been found which apparently do not follow them. Thus, Ba_2PrPtO_6 with both ions, Pt and Pr, with an identical oxidation state and not very different in size ($r_{Pr} = 0.85$ Å, $r_{Pt} = 0.625$ Å), presents an ordered distribution of ions over the octahedral site [20]. In this case, the size and charge differences criteria seem not to hold. According to Galasso [17], the ratio $\sigma = (r_{B'} - r_{B''})/r_{B'}$ determines the ordering in complex perovskite: if σ is greater than 0.09, the cationic distribution should be ordered. Although it is fulfilled in Ba_2PrPtO_6 ($\sigma = 0.11$), some of the perovskites studied here do not. Thus, for all the compounds studied in this paper, σ is greater than 0.09, and consequently all of them should be ordered. This is not what we observed. In fact, two situations have been found: those compounds with $\sigma > 0.33$ ($Ba(Y_{2/3}Mo_{1/3})O_3$ and $Ba(Y_{2/3}W_{1/3})O_3$) are ordered, whereas in $Ba(In_{2/3}Mo_{1/3})O_3$ and $Ba(In_{2/3}W_{1/3})O_3$ ($\sigma \sim 0.25$) both ordered and disordered structures seem to coexist. Indeed, the Ba- and In-containing oxides seem to present both distributions, random and ordered, though only for $Ba(In_{2/3}W_{1/3})O_3$ evidences were found of the existence of both forms. Probably, also an ordered form exists in the Mo-containing oxide though at room temperature only that with a random distribution was observed. Thus, by adjusting both the maximum temperature of treatment and the cooling rate, it could be possible to stabilise an ordered phase. Additional experimental work is under way on these and some other W(VI) and Mo(VI) complex perovskites to clarify this point. A different situation is found in the only Sr-containing oxide presented here, $Sr(In_{2/3}W_{1/3})O_3$. In this case, replacing Ba ($r = 1.61$ Å) by Sr ($r = 1.44$ Å) brings about a tilting of the octahedra to optimise some of the 12 ideally equal A–O bond distances, promoting a lowering of symmetry. This is a well-known size effect of Sr ion: the SrO_3 layers closely packed are distorted as a consequence of the small size of Sr(II) compared to oxide anions.

Finally, we would stress that, although the perovskite oxides are believed to be well understood, at least from a structural point of view, there are still many points remaining unclear. The geometrical and electrostatic picture of ionic compounds, has been useful for decades, but is clearly unsatisfactory; the complex perovskites studied in

Table 2
Selected inter-atomic distances (Å) in $A(B_{2/3}M_{1/3})O_3$ compounds

$Ba(In_{2/3}Mo_{1/3})O_3$		$Ba(In_{2/3}W_{1/3})O_3$ ordered		$Ba(In_{2/3}W_{1/3})O_3$ disordered		$Sr(In_{2/3}W_{1/3})O_3$		$Ba(Y_{2/3}Mo_{1/3})O_3$		$Ba(Y_{2/3}W_{1/3})O_3$	
Ba–O	$2.946(1)\times 12$	Ba–O	$2.940(9)\times 12$	Ba–O	$2.940(6)\times 12$	Sr–O(1)	3.14(1)	Ba–O	$3.006(8)\times 12$	Ba–O	$3.011(7)\times 12$
In/Mo–O	$2.083(1)\times 6$	In–O	$2.125(8)\times 6$	In/W–O	$2.079(8)\times 6$	–O(1)^{i}	3.10(2)	Y–O	$2.084(6)\times 6$	Y–O	$1.997(8)\times 6$
		In/W–O	$2.032(8)\times 6$			–O(1)^{ii}	$2.68(1)\times 2$	Y/Mo–O	$2.167(8)\times 6$	Y/W–O	$2.258(9)\times 6$
						–O(2)	$2.61(2)\times 2$				
						–O(2)^{i}	$2.57(2)\times 2$				
						–O(2)^{ii}	$3.05(2)\times 2$				
						–O(2)^{iii}	$3.37(2)\times 2$				
						W/In–O(1)	$2.060(2)\times 2$				
						–O(2)	$1.90(1)\times 2$				
						–O(2)^{i}	$2.26(1)\times 2$				

this work are examples of this. Nowadays, some other approaches to inorganic solids are being developed [21].

4. Concluding remarks

The usefulness of the Pechini method for preparing W(VI) and Mo(VI) complex perovskites has been shown in this work. $A(B'_{2/3}B''_{1/3})O_3$ (A = Ba or Sr; B' = In or Y; B'' = W or Mo) were obtained after firing the precursor powders for 8 h at 1200°C. The structure of these compounds was determined by combining HREM and XRD. Although the generally accepted criteria to predict the type of cation distribution, random or ordered, over the octahedral sites of complex perovskites indicate that the five oxides studied here should be ordered, electron diffraction and microscopy results revealed a different situation. Thus $Ba(In_{2/3}Mo_{1/3})O_3$, $Ba(In_{2/3}W_{1/3})O_3$ and $Sr(In_{2/3}W_{1/3})O_3$ were found to present a random distribution of In and W (or Mo). In $Ba(In_{2/3}W_{1/3})O_3$, two forms, ordered and disordered, coexist at room temperature. On the other hand, yttrium-containing oxides are ordered perovskites. These findings are one more example of the over-simplification inherent to the classical geometrical and electrostatic approach to inorganic solids. In particular, the perovskite structure has been widely studied and it is believed to be well understood; however, there is no satisfactory explanation even for its skeleton of corner-sharing octahedra. More elaborated explanations are being developed and successfully applied to complex compounds such as ternary aluminates [22].

Acknowledgments

This work was carried out with the financial assistance of CONACYT (Mexico) under Grant number 31198U.

References

[1] Y. Todate, J. Phys. Chem. Solids 60 (1999) 1173.
[2] T. Kolodiazhnyi, A. Petric, A. Belous, O. V'yunov, O. Yanchevskij, J. Mater. Res. 17 (2002) 3182.
[3] I.M. Reaney, R. Ubic, Ferroelectrics 228 (1999) 23.
[4] F.K. Patterson, C.W. Moeller, R. Ward, Inorg. Chem. 2 (1963) 196.
[5] A.A. Bokov, N.P. Protsenko, Z.-G. Ye, J. Phys. Chem. Solids 61 (2000) 1519.
[6] M.T. Anderson, K.B. Greenwood, G.A. Taylor, K.R. Poeppelmeier, Prog. Solid State Chem. 22 (1993) 197.
[7] R.S. Bhalla, HID lamp electrode comprising barium (yttrium or rare earth metal) tungstate or molybdate, Westinghouse Electric Corp., USA, US Patent 4152619, 1 May 1979.
[8] R.S. Bhalla, High-intensity vapor discharge lamp with sintering aids for electrode emission materials, Westinghouse Electric Corp., USA, US Patent 4152620, 1 May 1979.
[9] D. Harari, P. Poix, C. R. Acad. Sci. Paris Ser. C 276 (1973) 265.
[10] F. Sévéque, P. Delamoye, P. Poix, A. Michel, C. R. Acad. Sci. Paris Ser. C 269 (1969) 1536.
[11] M. Pechini, Method of preparing lead and alkaline-earth titanates and niobates and coating method using the same to form a capacitor, US Patent, No. 3330697, July 11, 1967.
[12] L.-W. Tai, P.A. Lessing, J. Mater. Res. 7 (1992) 502.
[13] J. Rodriguez-Carvajal, FULLPROF program, in: Abstracts of the Satellite Meeting on Powder Diffraction of the XVth Congress of the IUCr, Toulouse, France, 1990, p. 17.
[14] R.D. Shannon, Acta Crystallogr. A 32 (1976) 751.
[15] Y. Hikichi, S. Suzuki, Mater. Res. Bull. 22 (1987) 219.
[16] V.L. Balashov, L.N. Lykova, L.M. Kovba, A.A. Yevdokimov, Zh. Neorg. Khim. 30 (1985) 2132.
[17] F.S. Galasso, Structure Properties and Preparation of Perovskite-Type Compounds, Pergamon Press, Oxford, UK, 1970.
[18] PDF 26-0208, International Centre for Diffraction Data, Newton Square, PA, USA.
[19] A. Vegas, M. Vallet-Regi, J. González-Calvet, M.A. Alario-Franco, Acta Crystallogr. B 42 (1986) 167.
[20] U. Amador, C.J.D. Hetherington, E. Moran, M.A. Alario-Franco, J. Solid State Chem. 96 (1992) 132.
[21] A. Vegas, M. Jansen, Acta Crystallogr. B 58 (2002) 38.
[22] D. Santamaría, A. Vegas, The Zintl–Klemm concept applied to cations in oxides. I. The structures of ternary aluminates, private communication.